Journal of Alloys and Compounds 502 (2010) 195–198

Contents lists available at ScienceDirect

Journal of Alloys and Compounds

journal homepage: www.elsevier.com/locate/jallcom

TiN_x thin films for energy-saving application prepared by atmospheric pressure chemical vapor deposition

Xiaoxuan Lin, Gaoling Zhao*, Liqing Wu, Gangfeng Duan, Gaorong Han

State Key Laboratory of Silicon Materials & Department of Materials Science and Engineering, Zhejiang University, Hangzhou 310027, PR China

ARTICLE INFO

Article history:
Received 31 December 2009
Received in revised form 16 April 2010
Accepted 17 April 2010
Available online 16 May 2010

Keywords:
Titanium nitride
Non-stoichiometric
Atmospheric pressure chemical vapor deposition
Energy-saving application

ABSTRACT

Non-stoichiometric titanium nitride (TiN_x) thin films were fabricated on glass substrates by atmospheric pressure chemical vapor deposition (APCVD) using titanium tetrachloride and NH_3 as precursors. The relationships between x of TiN_x thin films and the structure, electrical and optical properties of films were investigated. The results showed that the crystalline property of over-stoichiometric films was better than that of sub-stoichiometric films. Electrical resistivity of films declined with increasing x from 0.83 to 1.25. Spectrophotometer curves of films demonstrated that the plasma wavelength (λ_p) shifted from the near-infrared region to the visible region and the peak value of transmittance increased with increasing x. The TiN_x thin film with $x = 1.25$ had low sheet resistance of 5 Ω/sq, high average reflectivity of 95% in the mid-far infrared region, 53% average reflectivity in the near-infrared region, and low average reflectivity of 10% in the visible region, indicating it can be a promising candidate as energy-saving films combining the function of solar control and low emission.

1. Introduction

Energy-saving coating glass has attracted special interests and has been used commercially in the architectural field. There are two dominating kinds of energy-efficient coatings. One is the solar control film; another is the low emission film. The solar control film reflects the near-infrared solar radiation which occupies about 50% the total solar radiation, while admitting natural light (daylight) [1,2]. It stops the solar energy entering into the building through the window in the hot climate region. The low emission (low-E) film has high reflectivity in the mid-far infrared region and limits its infrared radiation absorption of glass to reduce the emission of mid-far infrared radiation [3]. It has thermal insulating function and could be used in the cold climate region. Recently, more attention is attracted to a new type of energy-saving films which is suitable for hot summer and cold winter area in the architectural field. This new energy conserving film combines the function of solar control and low emission, which demands the combination of high infrared reflectivity and low sheet resistance. Usually, multilayer films are employed to the new energy-saving function in the current market. However, such multilayer films are complex and costly, and it would be more competitive to produce one-layer films with both solar control and low emission functions.

On the other hand, owing to the extreme hardness, high melting temperature, good corrosion and wear resistance, low electrical and thermal resistance, high thermal stability and golden color, titanium nitride (TiN) are widely applied as cutting tools, strengthening phases, diffusion barriers, electrical contacts and decorative coatings [4–8]. It also exhibits special optical performance such as high reflectivity at the red-end of the visible spectrum and low reflectivity near the ultraviolet region, which results in the golden appearance [9]. Recently, the potential of TiN thin films being used as new energy-saving coatings attracts wide attention. It is reported that the TiN film has been used as the solar control coating and the low emission coating on glass, respectively [10,11]. Furthermore, it is reported that the TiN_x film at high N/Ti ratio exhibits better solar control property [12], and the TiN_x film retains metallic property at N/Ti ratio as high as 1.3 [10]. Considering the metallic and solar control properties of TiN_x, its films can be expected to own the new energy-saving function. So far, only magnetron sputtering has been adopted to gain TiN_x films. Atmospheric pressure chemical vapor deposition (APCVD) is compatible with the float glass line. Therefore, it will be interesting to study APCVD preparation of TiN_x coating glass with both solar control and low emission functions.

In this paper, TiN_x thin films were prepared on glass substrates by APCVD. Effects of the chemical composition on the structure, optical, electronic and energy-saving properties of the TiN_x thin films were investigated.

2. Experimental

TiN_x thin films were deposited on glass substrates by APCVD under an inert atmosphere of N_2. The deposition temperature was set at 600 °C and the deposition time was kept at 1 min. The homemade experimental system which is similar to the reactor used in the Ref. [13] was a typical hot-wall reactor and the reactor

* Corresponding author. Tel.: +86 571 87952341; fax: +86 571 87952341.
E-mail address: glzhao@zju.edu.cn (G. Zhao).

0925-8388/$ – see front matter © 2010 Elsevier B.V. All rights reserved.
doi:10.1016/j.jallcom.2010.04.142

Table 1
Flow rate of precursors, lattice constant, thickness, sheet resistance and calculated reflectivity in the mid-far infrared region of the obtained TiN_x films.

X	Flow rate of precursors (sccm)			Lattice constant (nm)	Thickness (nm)	Sheet resistance (Ω/sq)	Calculated reflectivity in the mid-far infrared region (%)
	NH_3	N_2 (carrier gas)	N_2				
0.83	60	250	700	0.4182	242	234	19
0.92	68	250	700	0.4188	363	135	33
1.09	80	250	700	0.4205	264	70	53
1.13	78	300	622	0.4209	342	11	89
1.25	108	300	592	0.4200	442	5	95

chamber consisting of a horizontal silica tube set within a furnace. $TiCl_4$ (>98%) was preheated to 41.2 °C and then was carried into the reaction zone by N_2 gas from bubblers. High-purity grade (>99.999%) NH_3 and N_2 were used as the reactor gases. The reactor gases mentioned above were flowed through two tubes to the reaction zone separately. In the experiment, sub-stoichiometric ($x < 1$) TiN_x thin films were produced by changing the flow rate of NH_3 at a given relatively low flow rate of $TiCl_4$. Nitrogen-rich ($x > 1$) TiN_x thin films were deposited through increasing the flow rates of $TiCl_4$ and NH_3 with the same ratio between their flow rates. The detailed gas flow rate was listed in the Table 1.

The crystal phase were identified by X-Ray Diffraction (Rigaku model D/max-RA X-Ray Diffarctometer) using Cu-Kα ($\lambda = 0.1541$ nm) radiation operated at 40 kV to 80 mA. The thickness and surface morphology of films were studied by using Hitachi S-4800 filed emission scanning electron microscopy (SEM). The chemical component of films was analyzed by EDAX-FINDER 1000X Energy-dispersive X-ray (EDX) working at 20 kV. The sheet resistance was measured by XX-2 model four point probe system. Each sample was tested in three different positions and the average value was taken as the sheet resistance. The optical spectra were measured at room temperature by U-4100 UV–VIS–NIR spectrophotometer.

3. Results and discussion

3.1. Microstructure of TiN_x thin films

The chemical composition of TiN_x thin films obtained by changing the flow rate of precursor gases is listed in the Table 1. Fig. 1 shows the XRD patterns of TiN_x films. The presence of TiN in the NaCl structure is evident, and the obtained films are well crystallized with strong (2 0 0) diffraction peak near $2\theta = 43°$. The (2 0 0) orientation is due to the lowest surface energy in (2 0 0) plane which is the dominant contribution to the total energy [14]. It can be seen that the intensity of the peak increases when x increases from 0.83 to 1.13 and then decreases with further increasing x from 1.13 to 1.25. The film with $x = 1.13$ shows the strongest diffraction peak. For sub-stoichiometric TiN_x films, the low flow rate of the NH_3 (see Table 1) results in the low deposition rate, and leads to the decrease of the crystal property with decreasing x. When $x > 1$, the deposition rate sharply increases with increasing x, which is due to the increase of both reactor gases' concentration. So the crystal property sharply increases when x increases from 0.92 to 1.13. When flow rate of the NH_3 is too high, the ratio of $TiCl_4/NH_3$ becomes too small to get perfect TiN crystal. Therefore, crystallization phase decreases at $x = 1.25$. At the same time, it is observed that nitrogen-rich TiN_x thin films are better crystallized than sub-stoichiometric TiN_x thin films.

The lattice constant of the TiN_x thin film which is calculated from XRD pattern is given in the Table 1. The lattice constant of the TiN_x thin film increases with increasing x from 0.83 to 1.13. Then it declines with further increasing x from 1.13 to 1.25. The evolution of the lattice constant with stoichiometric can be ascribed to the defects' variety of TiN_x thin films. Refs. [15] and [16] have reported that N vacancies were formed in sub-stoichiometric TiN_x films, so the lattice constant increases with increasing x for sub-stoichiometric TiN_x films. On the other hand, Refs. [12] and [17] have reported that N interstitials and Ti vacancies could be formed in over-stoichiometric TiN_x films. The N interstitials cause the increase of the lattice constant, while the Ti vacancies result in the decrease of the lattice constant. For over-stoichiometric TiN_x films, when x increases, the concentration of N interstitials first increases and then reaches saturation. The Ti vacancies dominate the variety of the lattice constant during further increase of x. As a result, the lattice constant first increases and then decreases as x value increases for over-stoichiometric TiN_x films.

Fig. 2 shows SEM image of $x = 1.13$ sample. The morphologies of other samples are similar to that of $x = 1.13$ sample. The surface SEM images reveal that all films are homogeneous, continuous, flat and dense. It can be seen from the inserted cross-sectional SEM image that the film shows columnar grains. The thicknesses of the films, which were measured by the cross-sectional SEM image, are listed in Table 1.

3.2. Electrical properties of TiN_x thin films

The sheet resistance (R_s) of films is also listed in the Table 1. Using the thickness (d) data listed in Table 1, the electrical resis-

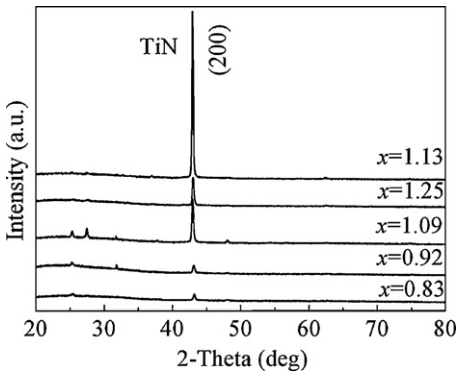

Fig. 1. X-ray diffraction patterns of TiN thin films with different chemical composition.

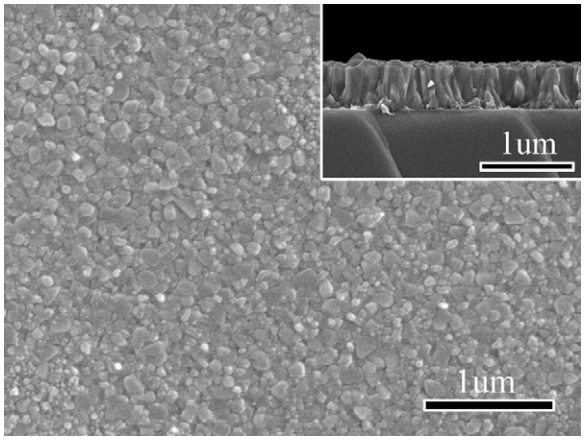

Fig. 2. SEM image of $TiN_{1.13}$ thin film prepared by APCVD. The inset shows the cross-sectional SEM of the film.

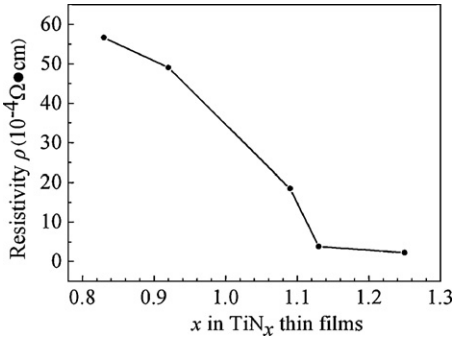

Fig. 3. The electrical resistivity of TiN_x thin films with various x.

tance (ρ) can be obtained according to the following equation:

$$\rho = R_s * d \quad (1)$$

Fig. 3 shows the evolution of electrical resistance with the N/Ti ratio. It can be seen that electrical resistivity decreases sharply when x increases from 0.83 to 1.13 and then decreases slightly with further increasing x. The electrical conductivity of TiN_x films is associated with the relaxation time of conduction electrons as the following [17]:

$$\rho = \frac{m^*}{\tau_D N e^2} \quad (2)$$

where N is the conduction electrons density, e is the electron charge, ρ is the resistivity, τ_D is the relaxation time of conduction electrons and m^* is the electrons effective mass. The variation of resistivity can be explained by the change of defects in TiN_x films and the alteration of the crystalline property, which will affect the conduction electrons density and the relaxation time of conduction electrons. The maximal τ_D value reaches at the stoichiometric composition [15]. In the case of $x < 1$, both the concentration of N vacancies and the τ_D value decline with increasing x, and the crystalline property increases sharply with increasing x. It has discovered that N vacancies and N interstitials whose role is the capture of electrons by the surface of Fermi could reduce the conduction electrons density [18]. Accordingly, the resistivity reduces sharply as x increases. In the case of $x > 1$, N interstitials and Ti vacancies are formed in super-stoichiometric TiN_x films. The τ_D value decreases with increasing x [15]. According to the Eq. (2), the variation of ρ is mostly due to the increasing concentration of free electrons. When $1 < x < 1.13$, the crystalline property increases sharply, leading to the sharp decrease of the resistivity. When $1.13 < x < 1.25$, the electrical resistivity decreases slightly with increasing x, which is due to the decrease of the crystalline property. It has reported that the increase of the nitride atoms concentration helps to reduce disorder so as to maintain good metallic character [10].

3.3. Optical and energy-saving properties of TiN_x thin films

Fig. 4(a) and (b) are the transmittance spectra and reflectivity spectra of TiN_x thin films, respectively. Fig. 4(a) reveals that TiN_x films show a transmittance band in the visible range (400–700 nm) and the transmittance increases with increasing x. Fig. 4(b) reveals that the reflectivity in the visible region of the sub-stoichiometric TiN_x film is larger than that of over-stoichiometric TiN_x films. The average reflectivity of $x = 0.83$ sample in the visible region is about 27%. While the average reflectivity of the $x = 1.13$ and $x = 1.25$ samples are 3% and 10%, respectively. The reflectivity in the near-infrared range increases with increasing x. When $x = 1.25$, the film exhibits about 53% average reflectivity in the near-infrared region, suggesting good solar control performance. It can be observed that there is a minimum reflectivity in the visible and the near-infrared

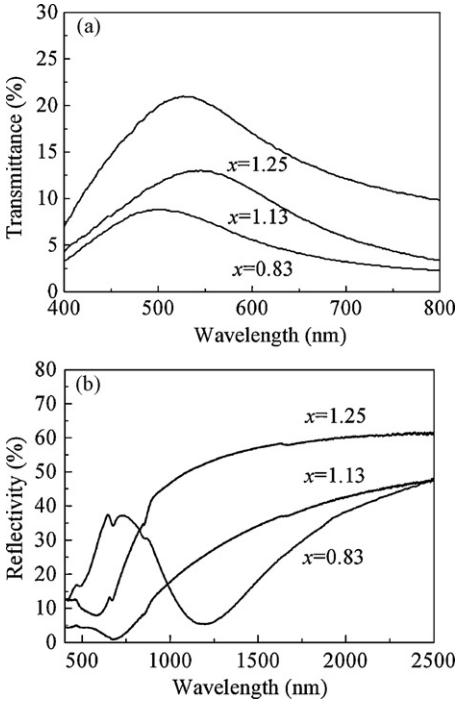

Fig. 4. Spectra of TiN_x thin films in visible-near-infrared region measured at room temperature: (a) transmittance spectra, (b) reflectivity spectra.

region. The reflectivity shows a sharp increase from this minimum point and then reaches a high value. For conductive films, this minimum point is called as the plasma wavelength (λ_p). From Fig. 4(b), it can be seen that the blue shift of the λ_p occurs as x increases. When x increases from 0.83 to 1.13, then to 1.25, the λ_p varies from about 1200 nm to 680 nm, then to 598 nm.

The blue shift of λ_p is related to the electrical conductivity, which can be explained by the following formula [19]:

$$\lambda_p = 2\pi c_0 \left(\frac{Ne^2}{\varepsilon_0 \varepsilon_1 m^*} - \gamma^2 \right)^{-1/2} \quad (3)$$

where N is the concentration of the free electrons, m^* is the conduction electron effective mass, ε_0 is the vacuum dielectric constant, ε_1 is the high-frequency dielectric constant, γ is the damping coefficient and e is the electronic charge. When x increases from 0.83 to 1.25, as discussed in Section 3.2, the concentration of free electrons increases, resulting the blue shift of λ_p. The blue shift of λ_p brings the low reflectivity in the visible region as shown in Fig. 4(b). Accordingly, the light pollution which exists in the sub-stoichiometric film ($x = 0.83$ sample) is avoided in over-stoichiometric TiN_x films ($x = 1.13$, and $x = 1.25$ samples). Also, as discussed above, over-stoichiometric TiN_x films show better solar control performance than sub-stoichiometric films.

Another important performance of new energy-saving films is the reflectivity in the mid-far infrared region, which is called as low-E property. The reflectivity of TiN_x films indicates a metallic behavior in the mid-far infrared region [17]. The reflectivity in the mid-far infrared region can be calculated by Drude equation [20] as following:

$$R_{IR} = (1 + 0.0053 R_s)^{-2} \quad (4)$$

where R_{IR} is the reflectivity in the mid and far infrared region and R_s is the sheet resistance of films. The calculated reflectivity in the mid-far infrared region, which is listed in the Table 1, is an average reflectivity in the whole wavelength of the mid-far infrared region. It can be found that more than 90% reflectivity in the mid-

far infrared region is obtained for films with $1.13 \leq x \leq 1.25$, which indicates that films with $1.13 \leq x \leq 1.25$ possess excellent low-E function.

Summarily, TiN_x films with $1.13 \leq x \leq 1.25$ have high reflectivity in the both near-infrared and mid-far infrared regions, which exhibits both solar control and low-E functions. Those super-stoichiometric TiN_x films also have low reflectivity in the visible region, avoiding the light pollution and have certain visible light transmittance. TiN_x films with higher transmittance in visible region are expected to further improve the properties of new energy-saving films. Researches are carrying out by doping suitable elements in TiN_x thin films to get thinner films with low sheet resistance.

4. Conclusions

Using the atmospheric pressure chemical vapor deposition (APCVD), non-stoichiometric TiN_x thin films were obtained on glasses. With increasing x value from 0.83 to 1.25, the sheet resistance reduced from 234 Ω/sq to 5 Ω/sq. At the same time, the visible transmittance and the reflectivity in the near-infrared region and the mid-far infrared region increased with increasing x. The plasma wavelength presented a blue shift with increasing the N/Ti ratio. When $x = 1.25$, the average reflectivity in the near-infrared region and the mid-far infrared region were about 53% and 95%, respectively. However, its transmittance in the visible region was only 24%, which need to be further improved. Over-stoichiometric TiN_x thin films can be a promising candidate as energy-saving films combining the function of solar control and low emission.

Acknowledgment

This work is supported by the National Natural Science Foundation of China (Grant Nos. 50672086 and 50372060).

References

[1] J.Y. Liu, Y.M. Lu, J. Liu, X.Y. Yang, X.B. Yu, J. Alloys Compd. (2010), doi:10.1016/j.jallcom.2010.01.053.
[2] P. Nitz, H. Hartwig, Sol. Energy 79 (2005) 573–582.
[3] J. Mohelnikova, Constr. Build. Mater. 23 (2009) 1993–1998.
[4] F. Akhtar, J. Alloys Compd. 459 (2008) 491–497.
[5] Q. Wang, Y. Li, J. Zhang, Y. Jin, D. Huang, S. Wu, Q. Cui, G. Zou, J. Alloys Compd. 494 (2010) L11–L14.
[6] T. An, M. Wen, L.L. Wang, C.Q. Hu, H.W. Tian, W.T. Zheng, J. Alloys Compd. 486 (2009) 515–520.
[7] Y. Xi, H. Fana, W. Liub, J. Alloys Compd. (2010), doi:10.1016/j.jallcom.2010.02.176.
[8] B. Song, Y. Yong, J. Mol. Struct. (THEOCHEM) 907 (2009) 74–84.
[9] Q.G. Zhou, X.D. Bai, X.Y. Xue, Y.H. Ling, X.W. Chen, J. Xu, D.R. Wang, J. Alloys Compd. 391 (2005) 141–145.
[10] G.B. Smith, A.B. David, P.D. Swift, Renew. Energy 22 (2001) 79–84.
[11] G.L. Zhao, T.B. Zhang, T. Zhang, J.X. Wang, G.R. Han, J. Non-Cryst. Solids 354 (2008) 1272–1275.
[12] G.B. Smith, P.D. Swift, Appl. Phys. Lett. 75 (1999) 630–632.
[13] N. Ramanuja, R.A. Levy, S.N. Dharmadhikari, E. Ramos, C.W. Pearce, S.C. Menasian, P.C. Schamberger, C.C. Collins, Mater. Lett. 57 (2002) 261–269.
[14] L.A. Cyster, D.M. Grant, K.G. Parker, T.L. Parker, Biomol. Eng. 19 (2002) 171–175.
[15] J.H. Kang, K.J. Kim, J. Appl. Phys. 86 (1999) 346–350.
[16] M. Tsujimoto, H. Kurata, T. Nemoto, S. Isoda, S. Terada, K. Kaji, J. Electron Spectrosc. Relat. Phenom. 143 (2005) 159–165.
[17] P. Patsalas, S. Logothetidis, J. Appl. Phys. 90 (2001) 4725–4734.
[18] M. Benhamida, A. Meddour, S. Zerkout, S. Achour, J. Mol. Struct. (THEOCHEM) 777 (2006) 41–44.
[19] S. Adachi, J. Appl. Phys. 87 (2000) 1264–1269.
[20] G. Frank, E. Kauer, H. Kostlin, Thin Solid Films 77 (1981) 107–117.